Mapping of Work Function in Self-Assembled V_2O_5 Nanonet Structures

Jeong Woo Park and Taekyeong Kim*

Department of Physics, Hankuk University of Foreign Studies, Yongin 17053, Korea.
*E-mail: tkim5562@gmail.com

ABSTRACT. We presented a mapping the work function of the vanadium pentoxide (V_2O_5) nanonet structures by scanning Kelvin probe microscopy (SKPM). In this measurement, the V_2O_5 nanonet was self-assembled *via* dropping the solution of V_2O_5 nanowires (NWs) onto the SiO_2 substrate and drying the solvent, resulting in the networks of V_2O_5 NWs. We found that the SKPM signal as a surface potential of V_2O_5 nanonet is attributed to the contact potential difference (CPD) between the work functions of the metal tip and the V_2O_5 nanonet. We generated the histograms of the CPD signals obtained from the SKPM mapping of the V_2O_5 nanonet as well as the highly ordered pyrolytic graphite (HOPG) which is used as a reference for the calibration of the SKPM tip. By using the histogram peaks of the CPD signals, we successfully estimated the work function of ~5.1 eV for the V_2O_5 nanonet structures. This work provides a possibility of a nanometer-scale imaging of the work function of the various nanostructures and helps to understand the electrical characteristics of the future electronic devices.

Key words: Scanning kelvin probe microscopy, Work function, V_2O_5 nanonet, Contact potential difference, Fermi level

INTRODUCTION

Transition metal oxides (TMO) including vanadium pentoxide (V_2O_5) have been widely used for the modern organic-based electronic devices such as organic light emitting diodes (OLED), organic photovoltaic (OPV) cells, field emission devices and photovoltaics due to their high quality electrical and optical properties.[1–7] For example, thermally deposited V_2O_5 thin film has recently been reported as charge transport layer in high-performance polymer organic field effect transistor (OFET).[8] In this case, the formation of V_2O_5 layer exhibited charge carrier mobility comparable to that of a pristine Au electrode, enabling the large-area and low-cost electronics. Another example is the three-dimensional structures of V_2O_5 nanosheets as electrodes in supercapacitors, which can be utilized for energy storage.[9] Although V_2O_5 have the exceptional properties, the surface potential measurements of V_2O_5 nanostructures remain challenging and have yet to be characterized experimentally in a nanoscale. Scanning Kelvin probe microscopy (SKPM) is very powerful tool to measure the contact potential difference (ΔV_{cpd}) between a metal tip and a sample surface for analyzing the local chemical potential distribution, surface charging, dopant concentration and work function of the various nanostructures.[10–15] Here, we measured the work function of the V_2O_5 nanonet structures on SiO_2 substrate by using SKPM techniques in ambient conditions, where the V_2O_5 nanonet structures were self-assembled

through dropping the V_2O_5 nanowire (NW) solution and dried the solvent on the substrate. SKPM based on an atomic force microscopy (AFM) maps the ΔV_{cpd} between the metal tip and the V_2O_5 nanonet. By generating the histograms of the ΔV_{cpd} obtained from the SKPM maps for the V_2O_5 nanonet as well as the HOPG as a reference for a calibration of the SKPM tip, we successfully estimated the work function of ~5.1 eV for the V_2O_5 nanonet structures.

EXPERIMENTAL

V_2O_5 NW solution was prepared by mixing 1 mg ammonium (meta) vanadate (Aldrich) with 10 mg acidic ion-exchange resin (DOWEX 50WX8-100, Aldrich) in 20 mL water as previous processes.[16,17] V_2O_5 NWs with lengths of a few micrometers were synthesized after keeping the solution for about 10–20 days. We dropped the V_2O_5 NW solution on the substrate and evaporated the solvent, leaving the V_2O_5 nanonet on the substrate which was a p-type degenerately doped Si wafer with 100 nm silicon oxide layer as shown in *Fig.* 1(a). *Fig.* 1(b) shows a schematic diagram of the SKPM experiments of the assembled V_2O_5 nanonet on the substrate. The SKPM measurements were performed by a commercial AFM based on a Park XE7 (Park Systems, Korea) in ambient conditions at room temperature. We used a Cr/Au coated tips (NCSTAu, Nanosensors) with a spring constant (k) of 7.4 N/m and a resonance frequency (ω_0) of 160 kHz to obtain the topography and ΔV_{cpd} images
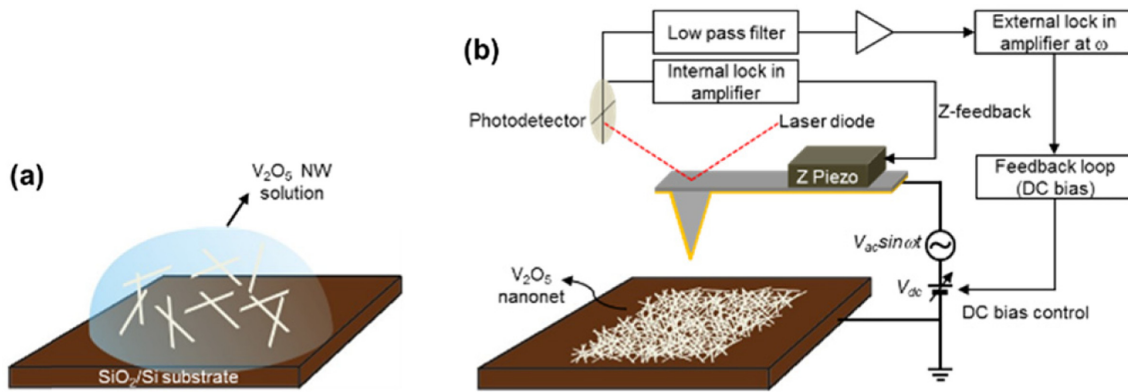
Figure 1. (a) Dropping the V$_2$O$_5$ NW solution on SiO$_2$ substrate. (b) Schematic diagram for SKPM setup. The tip scans over the V$_2$O$_5$ nanonet while oscillating at the resonance frequency of ω_0, in addition to the AC and the DC bias with the external lock-in amplifier which separates the ω frequency from the output signals. The surface potential is measured by reading the ω signal and the DC bias control in the feedback loop.

simultaneously in a non-contact mode. Electrical contacts to the substrate were grounded during the measurements.

We applied an AC modulation voltage ($V_{ac}\sin(\omega t)$) and a DC bias (V_{dc}) voltage between the metal tip and the V$_2$O$_5$ nanonet, and measured the ΔV_{cpd} by using an external lock-in amplifier (SR850, Stanford Research Systems) to analyze the amplitude of the tip oscillation. The tip oscillates due to the electrical force between the metal tip and the sample surface, where the ω component is separated from a whole output signal by the external lock-in amplifier. The total bias voltage between the tip and the V$_2$O$_5$ nanonet is

$$V(t) = V_{dc} - \Delta V_{cpd} + V_{ac}\sin(wt) \quad (1)$$

If we assume the tip-sample system as a parallel plate capacitor, the electrostatic force between the tip and the sample is given by:

$$F = -\frac{1}{2}V^2\frac{dC(z)}{dz}, \quad (2)$$

where C is a tip-sample capacitance and z is a tip-sample distance. The electrostatic force at a frequency ω, has the following expression

$$F_w = \frac{1}{2}\frac{dC}{dz}(V_{dc} - \Delta V_{cpd})V_{ac}\sin(wt) \quad (3)$$

This force is zero when the V_{dc} equals to the ΔV_{cpd}, so the DV_{cpd} can be measured by applying V_{dc} such that the oscillating amplitude at the frequency of ω is nullified by using the external lock-in amplifier that measures the w signal is zero in feedback loop.[11–13,18] In this case, we applied an AC modulation voltage amplitude (V_{ac}) of 1.5 V at a frequency (ω) of 17 kHz to the Au-coated tip.

RESULTS AND DISCUSSION

Fig. 2(a) shows the transmission electron microscope (TEM) images of V$_2$O$_5$ nanonet structures. The individual V$_2$O$_5$ NWs have the diameters of ~10−20 nm and the lengths of ~over 1 µm long as shown in previous results.[16,17] The V$_2$O$_5$ nanonet is randomly composed of the individual, bundles and stacked NWs. *Fig.* 2(b) shows the AFM topography image of the V$_2$O$_5$ nanonet on SiO$_2$ substrate. The thick NWs in the V$_2$O$_5$ nanonet indicate the bundle or stacked NWs after evaporation of the NW solution on SiO$_2$ substrate.

Fig. 3(a) is the expanded AFM topography image with various thicknesses of the V$_2$O$_5$ nanonet, corresponding to the white dashed square in *Fig.* 2(b). *Fig.* 3(b) is SKPM image obtained simultaneously with the topography image by measuring the local ΔV_{cpd} between metal tip and the V$_2$O$_5$ nanonet. The bottom graphs show the thickness (left) and the ΔV_{cpd} (right) profiles along the marked regions in each AFM topography and SKPM image. The entire sur-
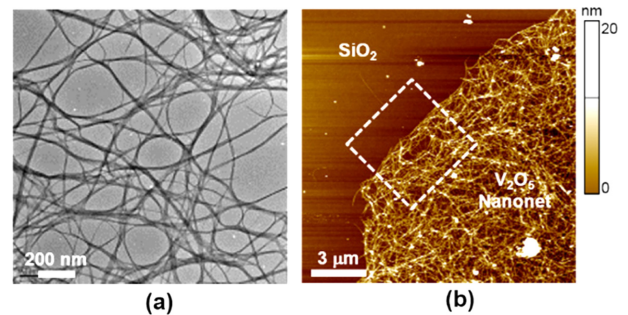

Figure 2. (a) TEM images of the V$_2$O$_5$ nanonet. (b) AFM topography image of the self-assembled V$_2$O$_5$ nanonet on SiO$_2$ substrate.
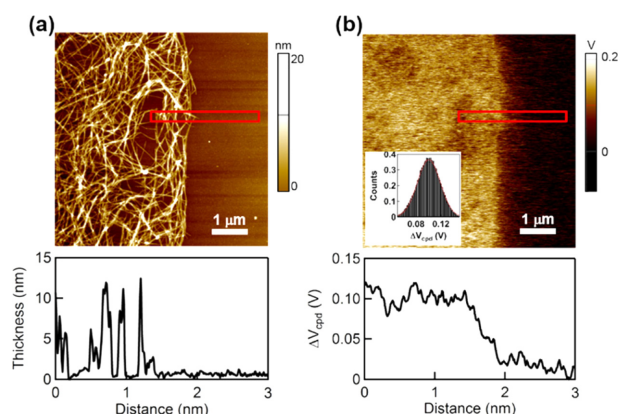
Figure 3. (a) and (b) AFM topography and corresponding SKPM images in the region of the white dashed square in Fig. 2(b). The thickness (gray) and the ΔV_{cpd} (red) profiles along the marked regions in AFM topography and SKPM image are shown in the bottom. Inset shows the statistical histogram for the ΔV_{cpd} in the region of V_2O_5 nanonet.
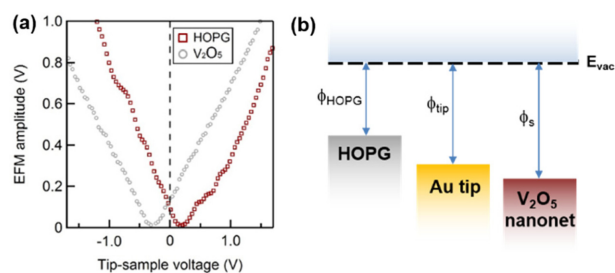

Figure 4. (a) EFM cantilever amplitude versus tip-sample bias voltage plots for the HOPG (gray) and the V_2O_5 nanonet surface (brown). (b) Representative band diagram for work functions of the HOPG, the Au tip, and the V_2O_5 nanonet. The black dashed line indicates the vacuum level energy.

face of cantilever (cone) which is coated with metal film also can be effected by the chemical potential from the sample, however only a few atoms at the end of the probe interact with the sample through attractive or repulsive forces. Therefore, the resolution of the topography image is higher than that of the SKPM image as shown in *Fig.* 3. In the SKPM image, the brightness variations come from the ΔV_{cpd} between the Au-coated tip and the sample surface. The bright region presents the smaller ΔV_{cpd} with respect to the Au-coated tip than the dark region, indicating smaller work function of V_2O_5 nanonet compare to that of the SiO_2.[19]

We calibrate the metal Au-coated tip with reference sample of HOPG to determine the work function of the SKPM tip (f_{tip}) that has been used in the experiments. The cantilever amplitude of the first harmonic (ω) signal is zero when the DC offset bias (V_{dc}) is equal to the surface potential of the sample surface. *Fig.* 4(a) shows the electric force microscopy (EFM) cantilever amplitude as a function of the tip-sample bias voltage relative to the HOPG substrate (gray) and the V_2O_5 nanonet (brown). As shown in the graph, the amplitude as the electrical force can be nullified if an applied external bias (V_{dc}) is equal to the ΔV_{cpd} that corresponds to the work function difference between the Au-tip and the sample.[13] The DC offset is about 0.15 V for the V_2O_5 nanonet (brown) and about −0.3 V for the HOPG surface (gray) as shown in the graph. Therefore, we could also obtain the work functions of the Au-tip and the V_2O_5 nanonet surface by using the two curves. The ΔV_{cpd} between the Au-coated tip and the HOPG is about −0.3 V, so the work function of the Au-tip is determined to be 4.95 eV

from the work function of the HOPG ($f_{HOPG} = 4.65$ eV) as a reference. Therefore, we can estimate the work function value (f_s) of the V_2O_5 nanonet surface by using the relation[13]

$$\Delta V_{cpd} = \frac{\phi_{tp} - \phi_s}{-e} , \qquad (4)$$

and it is found to be about 5.1 eV, which is almost same to the work function of the solution processed V_2O_5 film layer (~5.3 eV)[20,21] and a bit smaller value than the that of the V_2O_5 film layer, ~6.8 eV, which is fabricated in the ultra-high vacuum, results from the ultra-violet photoemission spectroscopy (UPS) and inverse photoemission spectroscopy (IPES) measurements.[5,22,23] The decreasing work function probably arise from the air exposure resulting in the shift of the photoemission onset towards lower binding energy due to an additional V^{4+} surface state, which is equivalent to a downwards shift of the vacuum level.[20] *Fig.* 4(b) shows the representative band diagram, depicting the work function values of the HOPG (f_{HOPG}), the Au tip (f_{tip}), and the V_2O_5 nanonet (f_s). It indicates that the V_2O_5 nanonet has higher work function than those of the HOPG and the Au tip.

CONCLUSION

In conclusion, we investigated the surface potential of the V_2O_5 nanonet by using SKPM technique in ambient conditions. We successfully obtained the work function of ~5.1 eV for the V_2O_5 nanonet by calibrating the Au-tip with reference sample of HOPG. This value is almost same to the work function of the solution processed V_2O_5 film layer measured by the UPS and IPES in the literature. This SKPM measurement allows us to evaluate the electronic properties of the V_2O_5 NW based devices in future.

REFERENCES

1. Shizuo, T.; Koji, N.; Yasunori, T. *J. Phys. D: Appl. Phys.* **1996**, *29*, 2750.
2. Reynolds, K. J.; Barker, J. A.; Greenham, N. C.; Friend, R. H.; Frey, G. L. *J. Appl. Phys.* **2002**, *92*, 7556.
3. Meyer, J.; Hamwi, S.; Bülow, T.; Johannes, H.-H.; Riedl, T.; Kowalsky, W. *Appl. Phys. Lett*. **2007**, *91*, 113506.
4. Kanno, H.; Holmes, R. J.; Sun, Y.; Kena-Cohen, S.; Forrest, S. R. *Adv. Mater.* **2006**, *18*, 339.
5. Meyer, J.; Hamwi, S.; Kröger, M.; Kowalsky, W.; Riedl, T.; Kahn, A. *Adv. Mater.* **2012**, *24*, 5408.
6. Zilberberg, K.; Trost, S.; Meyer, J.; Kahn, A.; Behrendt, A.; Lützenkirchen-Hecht, D.; Frahm, R.; Riedl, T. *Adv. Funct. Mater.* **2011**, *21*, 4776.
7. Glynn, C.; Creedon, D.; Geaney, H.; Armstrong, E.; Collins, T.; Morris, M. A.; Dwyer, C. O. *Sci. Rep.* **2015**, *5*, 11574.
8. Baeg, K.-J.; Bae, G.-T.; Noh, Y.-Y. *ACS Appl. Mater. Interfaces* **2013**, *5*, 5804.
9. Zhu, J.; Cao, L.; Wu, Y.; Gong, Y.; Liu, Z.; Hoster, H. E.; Zhang, Y.; Zhang, S.; Yang, S.; Yan, Q.; Ajayan, P. M.; Vajtai, R. *Nano Lett.* **2013**, *13*, 5408.
10. Yu, Y.-J.; Zhao, Y.; Ryu, S.; Brus, L. E.; Kim, K. S.; Kim, P. *Nano Lett.* **2009**, *9*, 3430.
11. Maragliano, C.; Lilliu, S.; Dahlem, M. S.; Chiesa, M.; Souier, T.; Stefancich, M. *Sci. Rep.* **2014**, *4*, 4203.
12. Rosenwaks, Y.; Shikler, R.; Glatzel, T.; Sadewasser, S. *Phys. Rev. B* **2004**, *70*, 085320.
13. Melitz, W.; Shen, J.; Kummel, A. C.; Lee, S. *Surf. Sci. Rep.* **2011**, *66*, 1.
14. Panchal, V.; Pearce, R.; Yakimova, R.; Tzalenchuk, A.; Kazakova, O. *Sci. Rep.* **2013**, *3*, 2597.
15. Cherniavskaya, O.; Chen, L.; Weng, V.; Yuditsky, L.; Brus, L. E. *J. Phys. Chem. B* **2003**, *107*, 1525.
16. Myung, S.; Lee, M.; Kim, G. T.; Ha, J. S.; Hong, S. *Adv. Mater.* **2005**, *17*, 2361.
17. Muster, J.; Kim, G. T.; Krstić, V.; Park, J. G.; Park, Y. W.; Roth, S.; Burghard, M. *Adv. Mater.* **2000**, *12*, 420.
18. Reddy, P.; Jang, S.-Y.; Segalman, R. A.; Majumdar, A. *Science* **2007**, *315*, 1568.
19. Choi, S.; Shaolin, Z.; Yang, W. *J. Korean Phys. Soc.* **2014**, *64*, 1550.
20. Zilberberg, K.; Trost, S.; Kahn, A.; Riedl, T. *Adv. Funct. Mater.* **2011**, *21*, 4776.
21. Gerardo, T.; Pampel, J.; Liracantu, M. *Energy Environ. Sci.* **2013**, *6*, 3088.
22. Meyer, J.; Zilberberg, K.; Riedl, T.; Kahn, A. *J. Appl. Phys.* **2011**, *110*, 033710.
23. Hancox, I.; Rochford, L. A.; Clare, D.; Sullivan, P.; Jones, T. S. *Appl. Phys. Lett.* **2011**, *99*, 013304.